Qualitative Comparison Between the Quantum Calculations and Electrospray Mass Spectra of Complexes of Polyammonium Macrotricyclic Ligands With Dicarboxylic Acids

C. Collette, D. Dehareng, E. De Pauw, and G. Dive
Université de Liège, 4000 Liège, Belgium

The host–guest interactions play a very important role in chemical and biological processes. It is therefore important to be able to characterize these complexes. Electrospray mass spectrometry can be used to characterize the complex formation. It provides information on the mass and the charge of these ionic complexes. In this article, we show that the use of ab initio and semiempirical calculations, in addition to the results obtained by electrospray mass spectrometry, reveal to be a promising tool for the study of these noncovalent complexes. In this article, host–guest complexes formed by macropolycyclic polyammonium host molecules and dicarboxylic acids are studied. (J Am Soc Mass Spectrom 2001, 12, 304–316) © 2001 American Society for Mass Spectrometry

The host–guest interactions play an important role in many biological processes [1]. Macrocyclic and macropolycyclic polyammonium synthetic molecules have been shown to model the natural receptors and to complex strongly and selectively a variety of inorganic and organic molecules by electrostatic interactions [1, 2]. The selectivity of the complexation depends on the substrate and the macrocycle host cavity sizes as well as on eventual specific interactions [3, 4]. The characterization of these complexes and the determination of stability constants have been first studied by NMR, polarography, and acid–base titration [3–6]. Since the introduction of soft ionization, mass spectrometry can also be used to study host–guest complexation using a few products and time [7–10]. The possibility of detecting multiply charged ions in electrospray mass spectrometry allows us to obtain complete information on the mass and the charge of the ionic species in the gas phase. In addition, electrospray mass spectrometry could maintain in the gas phase the interactions between dianions and the ligand, and the technique is therefore considered a suitable method for the detection of ionic species in solution [11–13]. The question remains open whether the intensities of the signal measured in electrospray mass spectrometry can be linked to the relative concentration of the complexes in solution [14, 15].

In a previous paper, we reported the analysis of the behavior of two tris-macrocycles amines (chart 1) with dicarboxylic substrates [$^{-}CO_2$–$(CH_2)n$–CO_2^{-}] by electrospray mass spectrometry [16]. Thanks to the soft ionization conditions, the electrospray source should allow the interactions between diacids and the ligand to be maintained in the gas phase. In this paper, we have reported the influence of dicarboxylic acid size (n = 1–4) and isomeric structures on the extent of complexation and the competition between two dicarboxylic anions of different size. Electrospray mass spectrometry provides information on the mass and the charge of these ionic complexes. Their relative stabilities in the gas phase can also be evaluated using tandem mass spectrometry. Despite this information, mass spectrometry tells nothing about the structure of the complex and the different sites of complexation and complementary techniques revealed.

Quantum chemistry calculations have already been used to model the reaction and complexation of several molecules [17, 18]. We also present here the application of the ab initio and semiempirical calculations on some conformations of the complex ions. Good agreement exists between the relative stabilities of the complexes and their mass spectrometric behavior. This tool brings some insights into the complex behavior in the gas phase. The electrospray mass spectrometry technique in conjunction with quantum chemistry calculations reveals to be a promising tool for the study of noncovalent complexes.

Address reprint requests to Dr. C. Collette, Laboratoire de Spectrométrie de Masse, Département de chimie générale et de chimie physique, Université de Liège, B-4000 Liege, Belgium. E-mail: c.collette@ulg.ac.be.

1044-0305/01/$20.00
PII S1044-0305(00)00228-2

Received July 3, 2000
Revised November 13, 2000
Accepted November 17, 2000

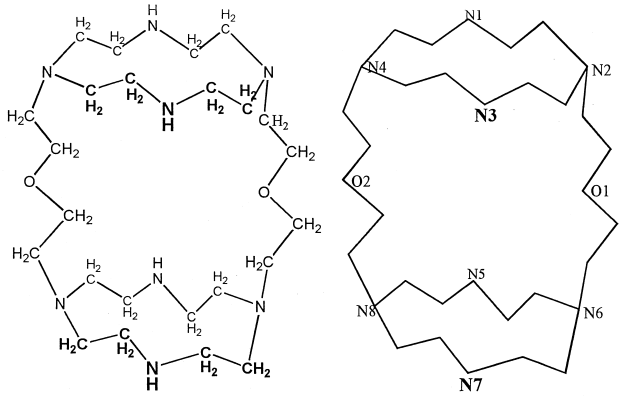

Diagram 1.

Materials and Methods

Theoretical Framework

The search for the lowest local minima of the potential energy hypersurface $E(Q)$, leading to the most stable conformers, is very complex work when the number of nuclear coordinate N is large. Very often, local minima are found and their relative stabilities are determined but it is rarely certain whether the global minimum is among the structures obtained.

For each local minimum found, the zero point energy (ZPE) should be added to its energy as well as corrections due to the effect of the temperature on the population of translational, rotational, and vibrational excited states, determined from the partition functions [19]. Thus the well-known thermal energies for translation and rotation are equal to $3/2\ RT$, the vibrational term being a more complex function of the frequencies. In addition to the energy terms, entropic ones are to be considered. They do not vary like the energetic ones. For instance, the translational entropy is the only term function of the pressure, of the form $R\ \ln(1/P)$. The translational and rotational entropies are less sensitive to the temperature than the vibrational one. The thermochemistry analysis will be performed for all of the minima at several values of the temperature and pressure. The ΔG thus derived is the value at the beginning of the reaction when all the species are the (T, P) conditions. Because this value must be zero at equilibrium, the more negative it is, and the more spontaneous the studied reaction is. The problem of calculating the frequencies for large complexes is a serious one. As a matter of fact, the optimization of such structures often leads to minima characterized by so small frequencies that their values become irrelevant, sometimes even null or imaginary. This problem is even more crucial when the frequencies are determined by numerical procedures, as it is the case in AM1 [20]. Thus, the matter of the impreciseness related to the problem will be addressed.

Because the object of this study is a series of complexes between a ligand ***L*** and one or several diacids ***Cn*** $HO_2C–(CH_x)_n–CO_2H$ ($x = 1, 2$), let us recall some energetic definitions. The interaction energy ΔE_{int} is the complex energy relative to the energy sum of its separate partners characterized by their *geometries in the complex*:

$$\Delta E_{int} = E(\text{optimized complex}) - E(\text{ligand } \boldsymbol{L}//\text{complex}) - \Sigma E(\text{diacids } \boldsymbol{Cn}//\text{complex}) \quad (1)$$

E being the total electronic energy as defined above, and often referred to as the internal energy, the term "//complex" means "at the geometry it has in the complex."

The complexation energy ΔE_{com} is the complex energy relative to the energy sum of its separate partners in *their optimized geometries*:

$$\Delta E_{com} = E(\text{optimized complex}) - E(\boldsymbol{L}//\text{opt.}) - \Sigma E(\boldsymbol{Cn}//\text{opt.}) \quad (2)$$

the term "//opt" means "at the geometry of the fully optimized most stable conformation." The difference between ΔE_{com} and ΔE_{int} is the deformation energy ΔE_{def} of the interacting entities:

$$\Delta E_{def} = E(\boldsymbol{L}//\text{complex}) + \Sigma\ E(\boldsymbol{Cn}//\text{complex}) - E(\boldsymbol{L}//\text{opt.}) - \Sigma\ E(\boldsymbol{Cn}//\text{opt.}) \quad (3)$$

The thermal energetic corrections $E_{th}(T)$ and the entropic ones $S(T,P)$ are added to the ZPE variation, ΔZPE, and to the ΔE_{com} in order to give a free energy term $\Delta G(T,P)$ depending on the temperature T and the pressure P:

$$\Delta G(T,P) = \Delta E_{com} + \Delta\text{ZPE} + \Delta E_{th}(T) - T\Delta S(T,P) \quad (4)$$

In the vacuum, the T and P effects are not considered and $\Delta G(T,P)$ is replaced by $\Delta E(\text{vac})$ which is the sum of the first two terms in eq 4.

Computational Tools

All the calculations were performed with GAUSSIAN94 [21], on two computers, a Dec 8400 with eight processors, and a Dec 4100 with four processors.

One neutral ligand cage was optimized at the HF level within the MINI-1′ basis set [22, 23]. Its electrostatic potential map was determined at the HF/MIN-1′ level. For all the systems, a full geometry optimization was performed at the semiempirical level AM1 [20]. One trimer complex was optimized at the DFT B3LYP [24] level, within the 6-31G basis set [25]. This calculation took 30 days in CPU time running in parallel on two processors of the Dec 4100 with 43 Megawords of central memory. In the following, these levels will be

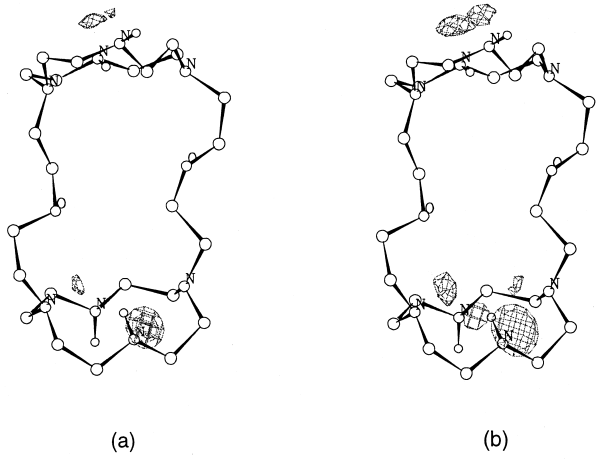

Figure 1. Neutral ligand optimized at the HF/MINI-1′ level, and EP contours at −100, −90, and −80 kcal/mol. No hydrogens are shown except those on the nitrogens.

referenced to as AM1 and B3LYP, respectively. The free energies are computed from the analytical frequencies through the usual statistical mechanics formulas [19].

One calculation in the solvent was performed using the self-consistent reaction field model labeled IPCM [26] (Isodensity Polarized Continuum Medium). This method is based on the PCM solvent model by Miertus et al. [27] and considers a cavity which is well fitted to the solute shape because it is defined by an electronic density isocontour chosen by the user. In this work, the relative dielectric constant and the isodensity contour were chosen, respectively, equal to 80 and 5×10^{-5} electron/bohr^3.

Building of the Cage Molecules and Their Complexes

The tris-macrocycle neutral ligand ***L*** initially considered was composed of two 12-membered saturated rings each containing four nitrogens, here called nitro-macrocycles, and linked together through two $–CH_2–CH_2–O–CH_2–CH_2–$ ether bridges attached to two opposite nitrogens (see chart 1). This molecule was constructed with the BUILDER module of the INSIGHT program [28].

This structure geometry was first optimized at the molecular mechanics level, using the classical force field CFF91 [29]. The result was the starting point for the geometry optimization at the HF/MINI-1′ level. In order to correctly chose the protonation sites, the electrostatic potential (EP) map of this optimized structure was calculated (Figure 1). The negative EP regions give a good indication of the proton affinity sites. The most negative potential value, around −100 kcal/mol, corresponds graphically to the most extended hatched region and is found near a secondary amine nitrogen which is N7 in chart 1. By reference to chart 1, a negative potential appears at −80 kcal/mol on N1, N8, and N3. From this result, the first protonation site can reasonably be considered on one of the secondary amine nitrogens, N7 for instance. For the biprotonated system, in order to decrease the electrostatic repulsion energy, the second proton will be located on the farthest opposite nitrogen N1. Two monoprotonated and biprotonated cage conformations were then optimized at the AM1 level. The two biprotonated structures were optimized with one proton on each macrocycle and are denoted ***2H1*** and ***2H2*** in the following; they differ by the torsions in the nitro-macrocyles. They are presented in Figure 2. Let us point out that ***2H2*** looks like the optimized neutral conformation. One of the monoprotonated ligand conformations looked like ***2H1*** and will be noted ***H1***. The other one does not resemble ***2H2*** and will therefore be noted ***H3***.

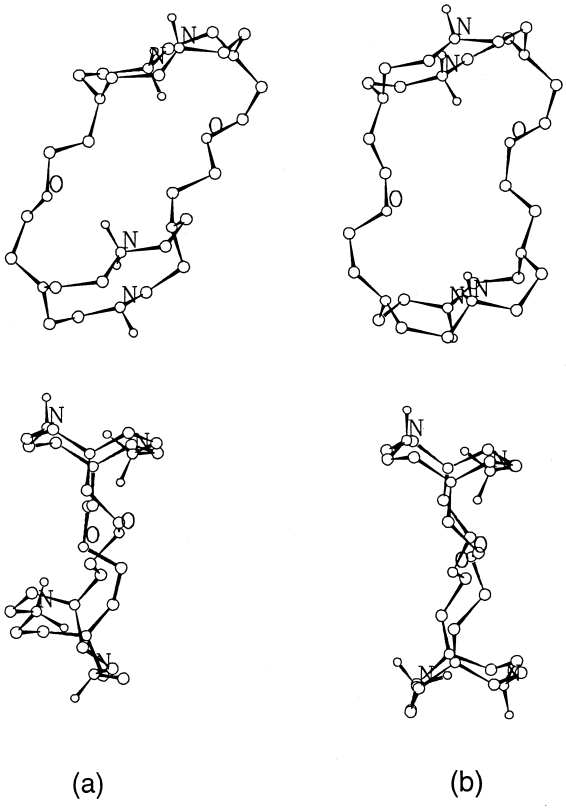

Figure 2. Biprotonated cages ***2H1*** (**a**) and ***2H2*** (**b**) whose geometries were optimized at the AM1 level. No hydrogens are shown except those on the nitrogens.

The complexes differ by their ligand conformation and protonation state, as well as by the relative position of the diacids(s) ***Cn***. The first characteristic will be referred to by the notation (***Hi***, i = 1,2), in relation with its resemblance with either ***2H1*** or ***2H2***. The protonation state (mono or bi) will be indicated by the number before the term ***Hi*** (***Hi*** or ***2Hi***). The following diacids were chosen: oxalic (***C0***), maleic (***C2m***), fumaric (***C2f***), and adipic (***C4***). Their chosen relative position in the complex was either in-between the rings and the ether bridges, labeled "***in***", or interacting outside one of the rings, labeled "***up***" or "***do***". Dimers, trimers, and

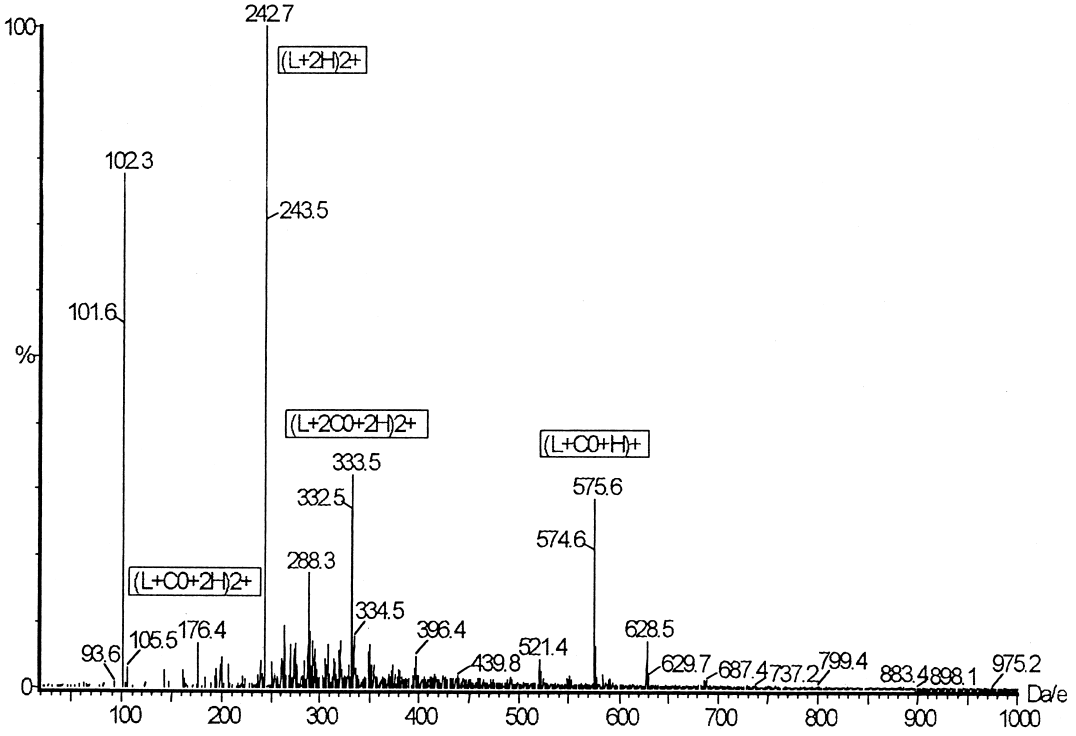

Figure 3. ESI positive ion mass spectrum of a solution of a 50/50 mixture of the tris-macrocycle ligand ***L*** and the oxalic acid ($n = 0$) in a solution of water/acetonitrile with formic acid. The voltage applied to the sampling cone was 7 V.

one tetramer were considered with ***C0*** and ***C4***. Only dimers were investigated for the maleic and fumaric acids.

The labels and the composition of the complexes are summarized in the Appendix.

Electrospray Mass Spectrometry Conditions

The synthesis of the macrocycle ***L*** and the solutions' conditions have been described previously [16]. Positive ESI mass spectra were obtained using a VG Platform (Micromass, Manchester, UK) quadrupole mass spectrometer. Samples were introduced in the ionization chamber at atmospheric pressure through a stainless steel capillary. The solvent used was water + formic acid. The flow was fixed at 0.02 mL/min. A gas flux (N_2) acts as nebulizing gas (15 L/h). The voltage difference applied between the capillary and the counterelectrode is 3 kV. A drying gas curtain is produced by a N_2 flow at 250 L/h. The ESI interface was heated to 80 °C. The voltage applied to the sampling cone was fixed at 7 V. Scanning was performed from *m/z* 200 to 1000 in 10 s. Positive ESI mass spectra MS/MS were obtained on a VG Quattro triple quadrupole mass spectrometer. The collision energy was fixed at 5 eV in the collision chamber and the pressure of the collision gas (Ar) was 5×10^{-3} mbar. Daughter ion scanning was obtained between *m/z* 80 and 900.

Experimental Results

Influence of the Length of the Dicarboxylic Acid on the Extent of Complexation

The positive ESI mass spectrum of a solution at pH7 containing equivalent concentration (2×10^{-3} M) of tris-macrocycle ***L*** and dicarboxylic acids [***Cn*** = HCO_2–$(CH_2)_n$–CO_2H], shows three peaks corresponding to complex formation between the ligand and the diacids (Figure 3). Two peaks correspond to dimers singly $(\boldsymbol{L} + \boldsymbol{Cn} + H)^+$ (for $n = 0$, *m/z* 576) and doubly charged $(\boldsymbol{L} + \boldsymbol{Cn} + 2H)^{2+}$ (for $n = 0$, *m/z* 288), one peak corresponds to a trimer doubly charged $(\boldsymbol{L} + 2\boldsymbol{Cn} + 2H)^{2+}$ (for $n = 0$, *m/z* 333). The spectrum with ***C0*** also contains one peak corresponding to the double protonation $(\boldsymbol{L} + 2H)^{2+}$ (*m/z* 243). For $n \neq 0$, peak corresponding to the monoprotonated ligand $(\boldsymbol{L} + H)^+$ is also observed.

Table 1 shows, for different sizes of dicarboxylic acids ($n = 0-4$), the ratio of complexed ions (C) on noncomplexed ions (NC). From these results, the size of the dicarboxylic acid has a large influence on the complexation yield. The peak intensities of the complex ions decrease when the size of the dicarboxylic acid increases and the tris-macrocycle ***L*** appears to have the best complementarity with oxalic acid. In addition, the number of protons required for the observation of the complex ions with one or two acids depends on the size of the dianions. In the case of oxalic acid, the most

Table 1. Relative abundances of ions corresponding to the complexed (C) and noncomplexed ligand (NC), in the positive spectra of solutions containing the ligand ***L*** and different dicarboxylic acid [***Cn*** = HCO_2–$(CH_2)_n$–CO_2H]

Complex	C/NC[a]
$(\boldsymbol{L} + \boldsymbol{C0} + H)^+$	0.3
$(\boldsymbol{L} + \boldsymbol{C0} + 2H)^{2+}$	0.1
$(\boldsymbol{L} + 2\boldsymbol{C0} + 2H)^{2+}$	0.4
$(\boldsymbol{L} + \boldsymbol{C1} + H)^+$	0.06
$(\boldsymbol{L} + \boldsymbol{C1} + 2H)^{2+}$	0.04
$(\boldsymbol{L} + 2\boldsymbol{C1} + 2H)^{2+}$	0.1
$(\boldsymbol{L} + \boldsymbol{C2} + H)^+$	0.03
$(\boldsymbol{L} + \boldsymbol{C2} + 2H)^{2+}$	0.02
$(\boldsymbol{L} + 2\boldsymbol{C2} + 2H)^{2+}$	0.03
$(\boldsymbol{L} + \boldsymbol{C4} + H)^+$	—
$(\boldsymbol{L} + \boldsymbol{C4} + 2H)^{2+}$	0.07
$(\boldsymbol{L} + 2\boldsymbol{C4} + 2H)^{2+}$	0.01

[a]C/CN denotes the ratio of the intensities of the indicated complex ion to the sum of the noncomplexed species.

Table 2. Relative abundances of ion corresponding to the complexed (C) and the noncomplexed ligand (NC) in the positive ion spectra of solutions containing the ligand ***L*** and two dicarboxylic acids (oxalic and adipic acids) (a) and the ligand ***L*** and each acid alone (b)

Complex	C/NC[a]
(a)	
$(\boldsymbol{L} + \boldsymbol{C0} + H)^+$	0.4
$(\boldsymbol{L} + \boldsymbol{C0} + 2H)^{2+}$	0.05
$(\boldsymbol{L} + 2\boldsymbol{C0} + 2H)^{2+}$	0.3
$(\boldsymbol{L} + \boldsymbol{C4} + H)^+$	0.01
$(\boldsymbol{L} + \boldsymbol{C4} + 2H)^{2+}$	0.5
$(\boldsymbol{L} + 2\boldsymbol{C4} + 2H)^{2+}$	0.2
$(\boldsymbol{L} + \boldsymbol{C0} + \boldsymbol{C4} + 2H)^{2+}$	0.7
(b)	
$(\boldsymbol{L} + \boldsymbol{C0} + H)^+$	0.3
$(\boldsymbol{L} + \boldsymbol{C0} + 2H)^{2+}$	0.1
$(\boldsymbol{L} + 2\boldsymbol{C0} + 2H)^{2+}$	0.4
$(\boldsymbol{L} + \boldsymbol{C4} + H)^+$	—
$(\boldsymbol{L} + \boldsymbol{C4} + 2H)^{2+}$	0.07
$(\boldsymbol{L} + 2\boldsymbol{C4} + 2H)^{2+}$	0.01

[a]C/NC denotes the ratio of the intensities of the corresponding complex ion to the sum of the noncomplexed ionic species.

intense signal is obtained for the associations $(\boldsymbol{L} + \boldsymbol{Cn} + H)^+$ and $(\boldsymbol{L} + 2\boldsymbol{Cn} + 2H)^{2+}$. For adipic acid, the biprotonated dimer $(\boldsymbol{L} + \boldsymbol{Cn} + 2H)^{2+}$ gives us the most intense signal. These observations set up a question: can the ligand complex the diacids at two sites? Each site depending on the dicarboxylate size.

There are different hypotheses to explain how the diacids are complexed by the ligand. One oxalic acid molecule can be complexed inside the cavity because of its size. The second diacid should then be complexed outside the cavity. In the case of adipic acid, complexation should preferentially occur only outside the cavity by the two carboxyl groups. In order to test the influence of the dicarboxylic acid size on the complexation selectivity, a solution containing two acids of different size (oxalic and adipic acids) with the ligand was analyzed. The spectrum shows six peaks corresponding to the complexation of each acid to form four dimers singly $(\boldsymbol{L} + \boldsymbol{Cn} + H)^+$ and doubly charged $(\boldsymbol{L} + \boldsymbol{Cn} + 2H)^{2+}$, and two trimers doubly charged $(\boldsymbol{L} + 2\boldsymbol{Cn} + 2H)^{2+}$. In addition, a new seventh peak was detected at *m/z* 361, corresponding to a doubly charged ion in which one oxalic acid and one adipic acid are complexed by the ligand $(\boldsymbol{L} + \boldsymbol{C0} + \boldsymbol{C4} + 2H)^{2+}$. Table 2 summarizes the ratio of complexed ions (C) to noncomplexed ions (NC) for the different complex ions observed in this spectrum. The observation of Table 2 shows that the most abundant complex ion is the mixed ion in which both oxalic and adipic acids are complexed $(\boldsymbol{L} + \boldsymbol{C0} + \boldsymbol{C4} + 2H)^{2+}$. Moreover, the complexation yield increases considerably for adipic acid upon mixing with oxalic acid [in particular the abundance of the $(\boldsymbol{L} + \boldsymbol{C4} + 2H)^{2+}$ ion strongly increases].

In the previous article [16], one explanation has been proposed to explain the increase of the complexation yield of adipic acid in the presence of oxalic acid. This explanation can be found in the gas phase dissociation of the mixed complex ion $(\boldsymbol{L} + \boldsymbol{C0} + \boldsymbol{C4} + 2H)^{2+}$ which could lose one oxalic acid to generate the ion $(\boldsymbol{L} + \boldsymbol{C4} + 2H)^{2+}$. To test this hypothesis, the mixed ion $(\boldsymbol{L} + \boldsymbol{C0} + \boldsymbol{C4} + 2H)^{2+}$ was submitted to collision induced dissociation (CID) after its selection in the first mass spectrometry stage of a triple quadrupole. The

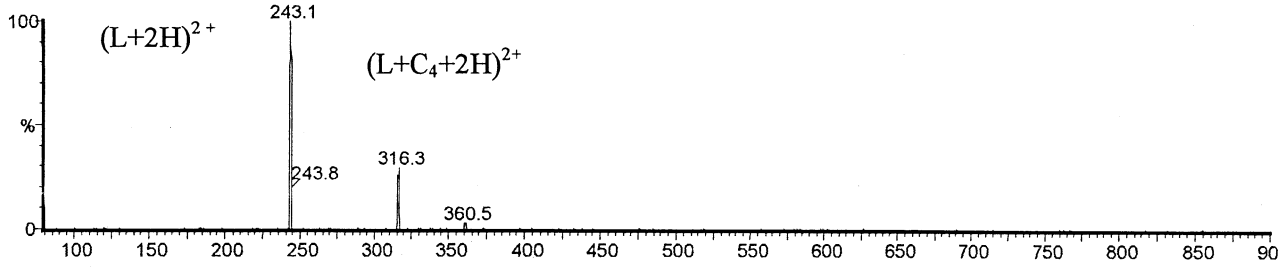

Figure 4. Fragment ion spectrum of the $(\boldsymbol{L} + \boldsymbol{C0} + \boldsymbol{C4} + 2H)^{2+}$ ion at 5 V/charge collision energy in a triple quadrupole.

fragment spectrum represented in Figure 4 shows two peaks corresponding to the dimer $(\boldsymbol{L} + \boldsymbol{C4} + 2H)^{2+}$ and the doubly charged free ligand $(\boldsymbol{L} + 2H)^{2+}$. This observation support the hypothesis of the formation of the ion $(\boldsymbol{L} + \boldsymbol{C4} + 2H)^{2+}$ in the gas phase from the loss of one oxalic acid from the trimer $(\boldsymbol{L} + \boldsymbol{C0} + \boldsymbol{C4} + 2H)^{2+}$. The preferential loss of one oxalic acid in the gas phase instead of one adipic acid puts doubt on the hypothesis of the complexation of the oxalic acid inside the cavity of the ligand. If the oxalic acid was complexed inside the cavity, why does it leaves the complex before the adipic acid? Perhaps the complementarity between the ligand and the substrate does not depend only on the size of the ligand cavity and on the length of the substrate, but also on some cooperative effects or on the rigidity of the ligand. In order to test the effect of the rigidity of the acid on the complexation, the next section shows the ESI mass spectra of two rigid *cis* and *trans* unsaturated diacids.

Isomeric Selectivity of the Complexation

Equimolar solutions of two unsatured isomeric diacids (maleic and fumaric acid) were mixed with the ligand ***L***, and analyzed by positive ion ESI. Figure 5 shows that only the *cis* isomer (maleic acid) can be complexed by the ligand ***L*** (Figure 5a). In the case of the *trans* isomer no complexation was observed. In this case, a full selectivity of the ligand for the *cis* isomer is observed but cannot be explain by mass spectrometry.

In the next part of the article we present quantum chemistry calculations which can bring some insights into the questions emerged from the mass spectrometry spectra.

Theoretical Results

Geometrical Considerations

The cage presents the shape of a tweezer pair able to rock around the ether bridges. The dimensions of the two "jaw"-like cavities are not the same because the distance N1–N5 and N3–N7 (chart 1) can be significantly different, as seen in the case of the biprotonated system (Figure 2). The vibrational motions related to the macrocyle and ether bridge conformational changes are characterized by very low frequencies. For instance, for the two AM1 optimized ***2Hi***, $i = 1, 2$, there are 11 or 12 frequencies lower than 100 cm^{-1} related with those deformations.

All the tertiary amine nitrogens linked to the ether bridges presents a very small pyramidalization, their lone pair being oriented toward the inside of the cavity. Thus, any proton put on one of them could not point to the exterior of the ligand cage.

As to the complexes, the position "***in***" of the ***Cn*** corresponds to an interaction between one ***L*** ether oxygen and one of the carboxylic hydrogens. With the maleic acid, a second ether–carboxylic interaction is observed because of the diacid folded conformation. For the oxalic and the adipic acids, secondary interactions occur between the second acidic function and the ligand but this is not observed for the fumaric acid. The position "***up***" can lead to a considerable deformation. For ***C0***, it consists in turning the two carbonyl oxygens face to face, i.e.,

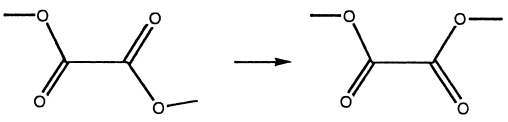

Diagram 2.

in order to present them both to the protonated nitromacrocyle. For ***C2f***, the acidic hydrogen is twisted by 180° away from the carbonyl oxygen, i.e.,

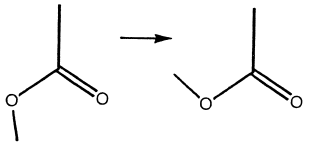

Diagram 3.

in order to avoid unfavorable contacts between the hydrogen and the ligand (Figure 6). For ***C2m*** and ***C4***, the deformation is related to the torsions of the backbone, in order to provide the best interaction with the ligand macrocycle.

Numerical Impreciseness on the Thermochemistry

For most systems involving the ligand ***L***, the lowest numerically derived AM1 frequencies were imaginary (one or two values) though the hessian did not present any negative eigenvalue. This is due to the numerical precision of the calculation. Two ways of determining the thermochemistry of the complex formation were then considered; either one neglects these imaginary frequencies in the vibrational $E_{th}(T)$ and $S(T,P)$ derivation or one transforms them into real ones. The difference between the two results is denoted err_{vim} in Table 3:

$$err_{vim} = E_{th}(\text{real } v) - TS(\text{real } v) - [E_{th}(\text{im } v) - TS(\text{im } v)] \quad (5)$$

Thus, apart from the error due to the harmonic approximation implicit to the statistical derivation of the vibrational partition function, there is an impreciseness of about 1–5 kcal/mol on the calculated thermic correction $E_{th}(T) - TS(T,P)$ due to numerical errors on the frequency determination. However, the various free energies are relative quantities, i.e., imply energy differences, for which a partial cancellation of errors

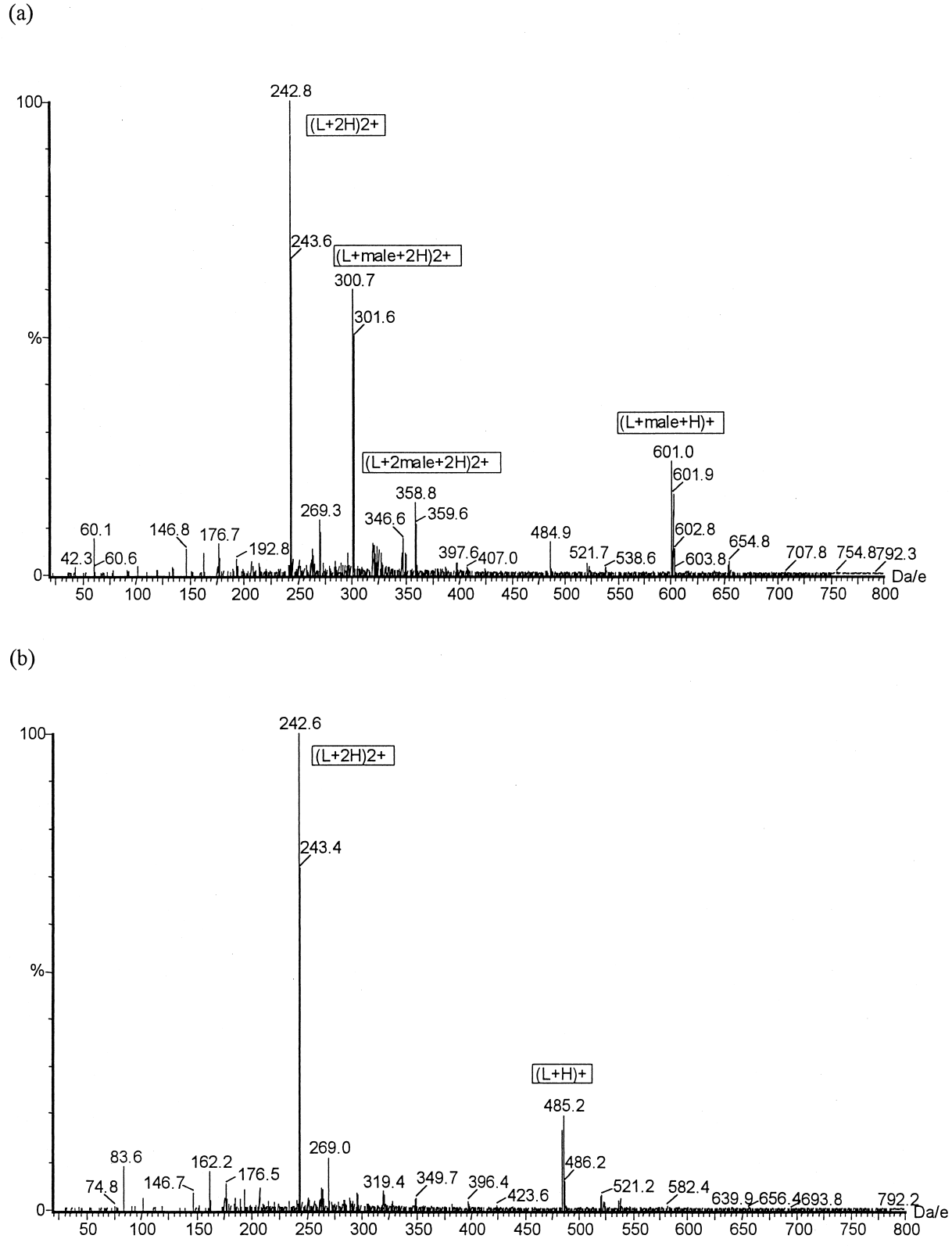

Figure 5. ESI positive ion mass spectra of (**a**) a solution of a 50/50 mixture of the tris-macrocycle ligand ***L*** and the maleic acid and (**b**) a solution of a 50/50 mixture of tris-macrocycle ligand ***L*** and the fumaric acid in a solution of water/acetonitrile with formic acid. The voltage applied on the sampling cone was 7 V.

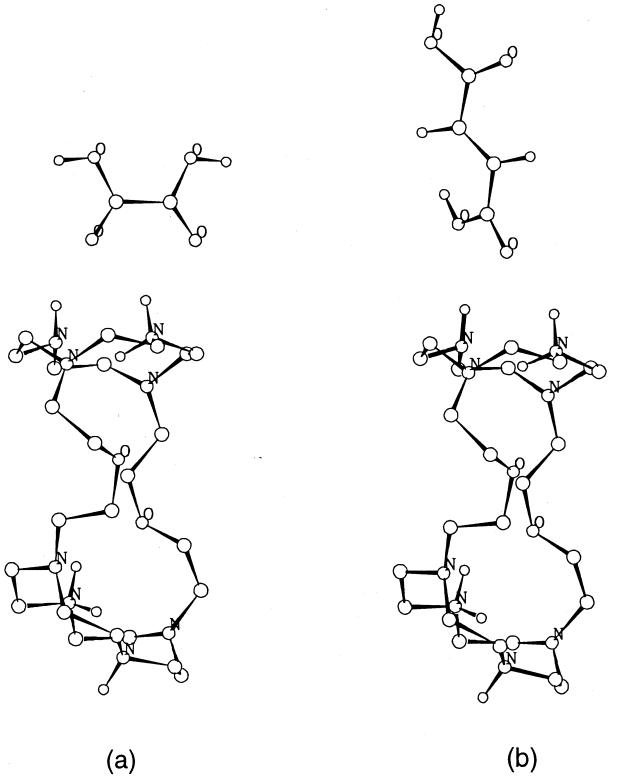

Figure 6. Biprotonated complex with the diacid in the "***up***" position: (**a**) ***C0*** and (**b**) ***C2f***.

happen. For instance, the impreciseness err_{vim} on the formation free energy of ***2H2 − C0up − C0in*** or ***2H2 − C4up − C0in*** is equal to 2.52 or −1.33 kcal/mol. These values are somewhat smaller than err_{vim}.

The Complexes Formation: Temperature and Pressure Effects

A pressure decrease from P_i to P_f always has an unfavorable influence on a complex formation, via the translational entropic term, $[R \ln(1/P_f) - R \ln(1/P_i)]$ for a dimer. On the contrary, a temperature decrease lowers all the entropic terms, and particularly the vibrational one, through the sensitive value of the partition functions. Tables 4 and 5 present the free formation energies $\Delta_f G$ calculated for several T and P conditions, for monoprotonated and biprotonated complexes. It appears, for instance, that the P decreases from 1 to 10^{-6} atm and can be compensated by a T lowering from 273 to 173 K because the $\Delta_f G$(C7) values lie in between the $\Delta_f G$(C1) and the $\Delta_f G$(C2) ones. The $\Delta_f G$ changes when passing from a monoprotonated to a biprotonated system are different for the ***up*** and the ***in*** dimers. For ***C0***, $\delta\Delta_f G$(***up***) = [$\Delta_f G$(***Hi − C0up***) − $\Delta_f G$(***2Hi − C0up***)] ranges from 5 to 7.5 kcal/mol, whereas $\delta\Delta_f G$(***in***) is much smaller, about 1 to 2 kcal/mol. The monoprotonated species do not favor the ***in*** or ***up*** position of the oxalic acid, whereas the biprotonated ones show a large preference for the ***up*** position. For ***C2m*** and ***C2f***, $\delta\Delta_f G$(***up***) ranges from 2 to 5 kcal/mol and $\delta\Delta_f G$(***in***) from −0.1 to −4 kcal/mol. These variations do not obey simple rules because several important terms are involved in the complexation, the interaction energy ΔE_{int} and the deformation energy ΔE_{def}. The first term is a favorable negative contribution but the second one is a positive unfavorable one. Some values of ΔE_{int} and ΔE_{def} are presented in Table 6. For instance, the interaction between $(LH_n)^{n+}$ and ***C2m*** in the "***in***" position is larger for the monoprotonated complex than for the biprotonated system by 2.5 kcal/mol. Similarly, this stronger interaction induces a greater deformation but ΔE_{def} only varies by 0.3 kcal/mol. The better interaction between the partners in ***H2 − C2min*** by reference to ***2H2 − C2min*** can be understood on the basis of the complexes geometry shown in Figure 7. In the biprotonated system, one ether oxygen is oriented toward the protonated nitrogen of the "***up***" macrocyle but this is not the case in the monoprotonated complex. In this latter case, the ether oxygen is more free for an interaction with the ***C2m*** carboxylic hydrogen. As to the ***xH2 − C2fin*** complexes, the interaction energy is somewhat higher for the biprotonated system but the deformation energy variation becomes more important.

Fumaric acid forms much less stable complexes than maleic acid. This is mainly due to its lower complexation energy ΔE_{com} with the ligand. On one hand, the interaction energy is smaller with ***C2f***. For instance, ΔE_{int}(***C2m,up***) = −23.1 kcal/mol, whereas ΔE_{int}(***C2f,up***) = −16.6 kcal/mol. This can be qualitatively explained by the fact that ***C2m*** has two interaction sites with the cage, due to its *cis* conformation, whereas ***C2f*** has only one. On the other hand, the deformation energy can be much higher for ***C2f***.

From Table 5, it is not possible to make any distinction between the trimer's formation. Tetramers are also obtainable under certain conditions but are obviously more sensitive to the pressure factor. Some (T,P) conditions, C5 and C6 for instance, are very unlikely to produce stable complexes. It also appears that the complexes with ***C2m*** are stable under most (T,P) conditions.

On the basis of the formation energies, one investigated monoprotonated complex with ***C2f***, ***H2 − C2fin***, is easier to form than ***H2 − C0up***. Nevertheless, all the other complexes involving ***C0*** are produced easier than ***H2 − C2fup***.

Table 3. Error err_{vim} (kcal/mol) due to the imaginary frequencies obtained in AM1 (see text), calculated at T = 298.15 K and P = 1 atm. The number n_{im} of imaginary frequencies obtained for each presented system is given in parentheses. The (first) imaginary frequency is given in cm^{-1}

Complex	err_{vim} (n_{im})	1st ν_{im}
2H1	−0.784 (1)	i55.02
2H2	−3.326 (2)	i59.91
2H2 − C0in	−2.405 (2)	i59.90
2H2 − C0up − C0in	−0.803 (1)	i53.38
2H2 − C0in − C0up	−2.315 (2)	i67.22
2H2 − C4up − C0in	−4.656 (3)	i70.78

Table 4. Free formation energies $\Delta_f G$, in kcal/mol, calculated at the AM1 level, at different temperature and pressure conditions, labeled Ci, i = 1,7 as follows: C1 = (T = 298.15 K, P = 1 atm), C2 = (T = 273.15 K, P = 1 atm), C3 = (T = 223.15 K, P = 1 atm), C4 = (T = 173.15 K, P = 1 atm), C5 = (T = 223.15 K, $P = 10^{-4}$ atm), C6 = (T = 223.15 K, $P = 10^{-6}$ atm), C7 = (T = 173.15 K, $P = 10^{-6}$ atm). The $\Delta_f E$(vac) is the sum of the complexation energy and the ZPE contribution (see text). In all the complexes, the cage is in its monoprotonated structure

		$\Delta_f G$(Ci)						
Complex	$\Delta_f E$(vac)	C1	C2	C3	C4	C5	C6	C7
H1 − C0up	−6.37	+5.92	+4.89	+2.83	+0.74	+6.91	+8.95	+5.49
H2 − C0up	−4.63	+9.53	+8.30	+5.84	+0.02	+9.93	+11.97	+8.13
H1 − C0in	−6.52	+7.37	+6.17	+3.78	+1.38	+7.86	+9.90	+6.13
H2 − C0in	−4.62	+8.34	+7.20	+4.95	+2.69	+9.03	+11.07	+7.45
H2 − C2mup	−13.95	−1.64	−2.65	−4.68	−6.75	−0.60	+1.44	−1.99
H2 − C2min	−16.68	−1.27	−2.57	−5.18	−7.81	−1.10	+0.94	−3.06
H2 − C2fup	−3.02	+10.92	+9.74	+7.35	+4.96	+11.44	+13.48	+9.71
H2 − C2fin	−8.71	+3.00	+2.06	+0.16	−1.78	+4.24	+6.29	+2.98

Relative Stability of the Complexes

Among the two optimized monoprotonated ligands, ***H3*** has the lowest internal energy; it is 1.38 kcal/mol lower than ***H1***. The ΔZPE correction is very small (−0.13 kcal/mol) as well as the thermic term $\Delta E_{th}(T) - T\Delta S(T,P)$ that lies around +0.3 to +0.8 kcal/mol for the range of (T,P) conditions. Among the two optimized biprotonated ligand, the most stable conformation is ***2H1***, which is 3.822 kcal/mol lower in internal energy than ***2H2***. The ΔZPE correction is also negligible (−0.053 kcal/mol) and the thermic term $\Delta E_{th}(T) - T\Delta S(T,P)$ very small, in the range of 0.03 to 0.4 kcal/mol for the selected (T,P) conditions. Tables 7 and 8 present the relative free energies of all the monoprotonated and biprotonated complexes. The lines with zeros appearing in the tables correspond to the most stable conformer of a group. For instance, the trimer with two oxalic acids was studied in four arrangements: ***2H1 − C0up − C0in***, ***2H2 − C0up − C0in***, ***2H2 − C0in − C0up***, ***2H1 − C0up − C0do***, the last one being the most stable. For the biprotonated dimers, all the arrangements with the diacid ***up*** are the most stable, by about 2 to 6 kcal/mol, except for the fumaric acid for which the difference between the ***up*** and ***in*** positions is very small.

Tables 7 and 8 emphasize that there can be several energetically accessible complex arrangements. It is not possible to investigate all these structures and this study is focused on a few of them.

Interaction Energies

In all the investigated biprotonated complexes, the interaction between the ***C0*** in the "***up***" position and its

Table 5. Free formation energies $\Delta_f G$, in kcal/mol, calculated at the AM1 level, at different temperature and pressure conditions, labeled Ci, i = 1,7 as follows: C1 = (T = 298.15 K, P = 1 atm), C2 = (T = 273.15 K, P = 1 atm), C3 = (T = 223.15 K, P = 1 atm), C4 = (T = 173.15 K, P = 1 atm), C5 = (T = 223.15 K, $P = 10^{-4}$ atm), C6 = (T = 223.15 K, $P = 10^{-6}$ atm), C7 = (T = 173.15 K, $P = 10^{-6}$ atm). vac means $\Delta_f E$(vac) and is the sum of the complexation energy and the ZPE contribution (see text). In all the complexes, the cage is in its biprotonated structure

	(T,P) conditions							
Complex	vac	C1	C2	C3	C4	C5	C6	C7
2H1 − C0up	−12.21	−0.53	−1.47	−3.38	−5.32	+0.70	+2.75	−0.57
2H2 − C0up	−9.66	+1.17	+0.29	−1.47	−3.27	+2.62	+4.66	+1.49
2H1 − C0in	−7.55	+5.62	+4.51	+2.28	+0.04	+6.37	+8.41	+4.79
2H2 − C0in	−6.29	+6.93	+5.81	+3.58	+1.34	+7.67	+9.71	+6.09
2H2 − C2mup	−18.54	−7.45	−8.35	−10.14	−11.98	−6.06	−4.01	−7.23
2H2 − C2min	−14.51	−1.22	−2.31	−4.51	−6.73	−0.42	+1.62	−1.98
2H2 − C2fup	−5.78	+6.95	+5.87	+3.72	+1.55	+7.81	+9.85	+6.31
2H2 − C2fin	−5.75	+7.05	+5.97	+3.82	+1.65	+7.90	+9.95	+6.40
2H2 − C4up	−10.03	+2.18	+1.22	−0.76	−2.78	+3.32	+5.36	+1.97
2H2 − C4in	−8.34	+4.90	+3.88	+1.75	−0.43	+5.84	+7.88	+4.32
2H1 − C0up − C0in	−19.21	+4.96	+3.01	−0.94	−4.95	+7.23	+11.31	+4.55
2H2 − C0up − C0in	−18.32	+4.28	+2.46	−1.22	−4.97	+6.95	+11.03	+4.54
2H2 − C0in − C0up	−17.65	+7.03	+4.99	+0.90	−3.25	+9.06	+13.15	+6.26
2H1 − C0up − C0do	−21.24	+1.88	−0.01	−3.83	−7.70	+4.34	+8.42	+1.81
2H2 − C4up − C4in	−20.77	+3.09	+1.31	−2.44	−6.31	+5.72	+9.91	+3.19
2H2 − C4up − C0in	−19.54	+6.24	+4.15	−0.13	−4.46	+8.04	+12.12	+5.05
2H2 − C4in − C0up	−19.12	+3.88	+2.11	−1.57	−5.34	+6.60	+10.68	+4.17
2H2 − C4up − C4in − C0do	−28.79	+4.89	+2.37	−2.91	−8.35	+9.35	+18.47	+5.91

Table 6. Interaction ΔE_{int} and deformation ΔE_{def} energies (kcal/mol) calculated for the AM1 optimized complexes, at the AM1 level. For the trimer and tetramer complexes, dimer interactions were also considered, depending on the way to group, in parentheses, the partners

Interacting partners	ΔE_{int}	ΔE_{def}
H1 − C0up	−13.54	+6.55
H2 − C0up	−11.88	+6.47
H1 − C0in	−9.26	+2.28
H2 − C0in	−12.12	+6.60
H2 − C2mup	−18.84	+3.57
H2 − C2min	−23.35	+5.18
H2 − C2fup	−11.72	+7.54
H2 − C2fin	−10.34	+0.65
2H1 + C0up	−16.85	+3.86
2H2 + C0up	−16.70	+6.16
2H1 + C0in	−9.67	+1.45
2H2 + C0in	−11.72	+4.53
2H2 + C2mup	−23.11	+3.57
2H2 + C2min	−20.82	+4.88
2H2 + C2fup	−16.64	+10.11
2H2 + C2fin	−11.13	+4.44
2H2 + C4up	−25.06	+14.34
2H2 + C4in	−22.97	+13.48
(***2H1 − C0in***) + ***C0up***	−16.05	/
(***2H1 − C0up***) + ***C0in***	−8.49	/
2H1 + C0up + C0in	−25.29	+4.56
(***2H2 − C0in***) + ***C4up***	−24.67	/
(***2H2 − C4up***) + ***C0in***	−10.97	/
2H2 + C0in + C4up	−36.03	+15.03
(***2H2 − C0up***) + ***C4in***	−20.83	
(***2H2 − C4in***) + ***C0up***	−15.78	
2H2 + C0up + C4in	−37.01	+16.14
(***2H2 − C4up***) + ***C4in***	−20.59	
(***2H2 − C4in***) + ***C4up***	−24.42	
2H2 + C4up + C4in	−45.52	+22.99
(***2H2 − C4in − C4up***) + ***C0do***	−10.37	
(***2H2 − C4in − C0do***) + ***C4up***	−24.17	
(***2H2 − C4up − C0do***) + ***C4in***	−19.47	
2H2 + C4in + C4up + C0do	−56.20	+24.68

partner, be it the ligand alone ***2Hi*** or a dimer (***2Hi − Cn***), is characterized by a ΔE_{int} of about −16 to −17 kcal/mol (Table 6). For the ***C0*** in the "***in***" position, the ΔE_{int} range is somewhat larger, about −9 to −12 kcal/mol, the mean value being smaller than for the "***up***" position. The same tendency is observed for ***C4***, the ΔE_{int}("***up***") ranging from −24 to −25 kcal/mol and the ΔE_{int}("***in***") from −19 to −23 kcal/mol. The deformation energies are greater for the systems involving ***C4***, about 8 to 10 kcal/mol larger than for ***C0***. Finally, the complexation energies ΔE_{com} are −12.99, −10.54, and −10.72 for the dimers ***2H1 − C0up***, ***2H2 − C0up***, and ***2H2 − C4up***, respectively, and −8.22, −7.19, and −9.49 kcal/mol for the dimers ***2H1 − C0in***, ***2H2 − C0in***, and ***2H2 − C4in***, respectively. For the mixed trimer formation, if ***C4*** is put in the "***up***" position ***C0*** will be at the "***in***" one and vice versa. Thus, on a qualitative level, one should compare the ΔE_{com} for ***2H2 − C4up*** and ***2H2 − C0in*** on one hand, and that for ***2H2 − C4in*** and ***2H2 − C0up*** on the other hand. In the first case, ***C4*** is better attached to the ligand than ***C0*** by 3.53 kcal/mol; in the second case, ***C0*** is more tightly linked than ***C4*** by 1.05 kcal/mol. On a more quantitative level, partial dissociation free energies $\Delta_d G$ are calculated and presented in Table 9 for the two mixed trimers ***2H2 − C4in − C0up*** and ***2H2 − C4up − C0in***. These results reinforce the qualitative point of view: when ***C4*** is ***up*** and ***C0in***, ***C0*** leaves the complex first but the situation is reversed if ***C4*** is ***in*** and ***C0up***. Let us point out that the trimer ***2H2 − C4in − C0up*** is slightly more stable than ***2H2 − C4up − C0in*** (Table 8).

AM1 Versus Ab Initio Comparisons

The trimer ***2H1 − C0up − C0in*** was optimized at the DFT B3LYP/6-31G level, starting from the AM1 optimized geometry. The interaction energies were calculated at the B3LYP level, for the AM1 and B3LYP optimized geometries, and compared with the AM1 interaction energies. Interactions energies for the monoprotonated dimers ***H2 − C0in*** and ***H2 − C2fin*** were also calculated at the AM1 optimized geometries within the RHF/MINI-1′ level. The results are presented in Table 10.

At the frozen AM1 geometry, the interaction energy is always more important, from 1.5 to 4.3 kcal/mol by dimer interaction, except for ***H2 − C2fin***. Thus, all the previous AM1 ΔE_{int} and their related quantities (ΔE_{com},ΔG) should be more negative or less positive, except for the monoprotonated complex with ***C2f***. Moreover, the geometry has also a large influence on ΔE_{int}, particularly for the dimer interaction (***2H1 − C0up***) − ***C0in***. In the trimer, the ***C0*** are closer to the ligand and, in position "***in***", several distances become significantly smaller inducing much more negative ΔE_{int}. Thus, it must be kept in mind that the AM1 results are qualitative.

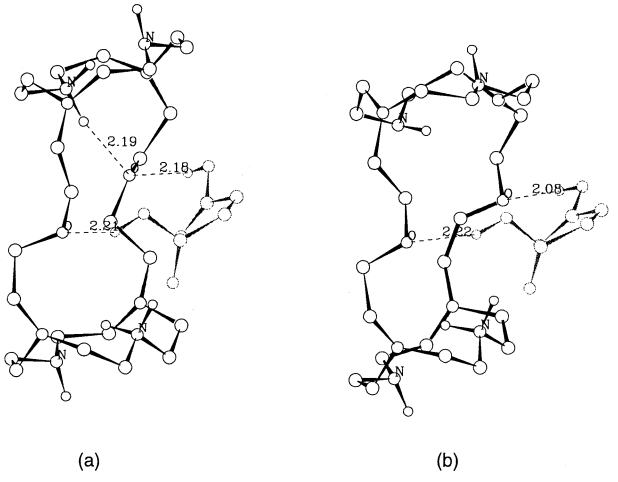

Figure 7. (**a**) Biprotonated and (**b**) monoprotonated complex with ***C2m*** in the position "***in***".

Table 7. Relative free energies $\Delta_r G$, in kcal/mol, calculated at the AM1 level, at different temperature and pressure conditions, labeled Ci, i = 1, 4 (see Table 4). In all the complexes, the cage is in its *monoprotonated* structure

Complex	$\Delta_r E$(vac)	$\Delta_r G$(C1)	$\Delta_r G$(C2)	$\Delta_r G$(C3)	$\Delta_r G$(C4)
H1 − C0up	0.0	0.0	0.0	0.0	0.0
H2 − C0up	1.73	3.61	3.41	3.01	2.64
H1 − C0in	−0.15	1.45	1.28	0.95	0.64
H2 − C0in	1.74	2.42	2.31	2.12	1.95
H2 − C2mup	+2.74	−0.37	−0.08	+0.50	+1.06
H2 − C2min	0.0	0.0	0.0	0.0	0.0
H2 − C2fup	+5.68	+7.93	+7.67	+7.19	6.73
H2 − C2fin	0.0	0.0	0.0	0.0	0.0

Comparison Between Theorical Results and Mass Spectra

Quantum chemistry calculations allow us to propose different stable geometries for the different complex ions observed in mass spectrometry. The stabilities of the complexes depend on the temperature and pressure conditions. In view of the calculation level used (semiempirical AM1 level), the values of the complex stabilities provide qualitative information about different proposed geometries. To compare the relative stabilities of the complexes, one also needs to know the experimental conditions to which the ions are submitted in the mass spectrometer. The problem is that, during the mass analysis, the ions undergo different conditions of pressure and temperature. Indeed, in the electrospray source, the ions are for the first time nebulizing in a region of atmospheric pressure and the second time are transported to the analyzer through a region of decreased pressure ($P_{atm} \rightarrow 10^{-6}$ atm). Nevertheless, the quantum calculations allow us to deduce some general informations on the complex ions geometries and their relative stabilities.

The most striking agreement between the calculations and the experiments concerns the different behavior of the ***C2m*** and ***C2f*** complexes. It is clear, either from the $\Delta_f G$ or from the ΔE_{com}, that ***C2m*** forms very stable associations with the ligand, whereas ***C2f*** does not. The parallel with experiment is direct because no complex with ***C2f*** is observed. The low value of ΔE_{com} for ***C2f*** comes either from the smallness of ΔE_{int} or from an important ΔE_{def}. In contrast to the ***C2m*** complexes, the low interaction energy for the ***C2f*** ones can be explained by the fact that ***C2f*** has only one site of interaction with the ligand, instead of two for ***C2m***. However, the theoretical results predicts monoprotonated complexes with ***C2f*** nearly as stable as some with ***C0***. This is in apparent contradiction with the experimental results: no monoprotonated complexes are observed for ***C2f***, whereas these are abundant for ***C0***. One can invoke several explanations to this discrepancy. First of all, the whole set of possible conformations is far from having been investigated in this work. It could happen that the number of energetically favorable complexes with ***C0*** was much greater than that with ***C2f***. Moreover, it must be kept in mind that the results are qualitative, not quantitative.

This argumentation is also to be invoked to explain the relative abundances of monoprotonated and biprotonated dimer complexes with ***C0***, which do not experimentally correspond to the calculated $\Delta_f G$ (Tables 4 and 5). As far as the biprotonated dimer and trimer complexes with ***C0*** are concerned, it appears from Table

Table 8. Relative free energies $\Delta_r G$, in kcal/mol, calculated at the AM1 level, at different temperature and pressure conditions, labeled Ci, i = 1, 4 (see Table 4). In all the complexes, the cage is in its biprotonated structure

Complex	$\Delta_r E$(vac)	$\Delta_r G$(C1)	$\Delta_r G$(C2)	$\Delta_r G$(C3)	$\Delta_r G$(C4)
2H1 − C0up	0.0	0.0	0.0	0.0	0.0
2H2 − C0up	2.55	1.69	1.77	1.91	2.06
2H1 − C0in	4.66	6.15	5.98	5.66	5.36
2H2 − C0in	5.92	7.45	7.28	6.96	6.66
2H2 − C2mup	0.0	0.0	0.0	0.0	0.0
2H2 − C2min	4.04	6.22	6.02	5.63	5.24
2H2 − C2fup	0.0	0.0	0.0	0.0	0.0
2H2 − C2fin	0.03	0.10	0.10	0.10	0.10
2H2 − C4up	0.0	0.0	0.0	0.0	0.0
2H2 − C4in	1.69	2.72	2.65	2.52	2.34
2H1 − C0up − C0in	2.03	3.08	3.02	2.89	2.74
2H2 − C0up − C0in	2.92	2.40	2.47	2.61	2.73
2H2 − C0in − C0up	3.58	5.15	5.01	4.73	4.44
2H1 − C0up − C0do	0.0	0.0	0.0	0.0	0.0
2H2 − C4up − C0in	0.0	0.0	0.0	0.0	0.0
2H2 − C4in − C0up	0.43	−2.36	−2.04	−1.44	−0.88

Table 9. Free energies $\Delta_d G$, in kcal/mol, for the dissociation of two trimers ***2H2 − Cn − Cn′*** into (***2H2 − Cn***) and ***Cn′***, ***Cn***, ***Cn′ = C0***, ***C4***. The (*T*,*P*) conditions are denoted as C*i* (see Table 4). A negative value means that the dissociation will proceed spontaneously. For comparison, the results for ***2H1 − C0up − C0do*** are also given

	(*T*,*P*) conditions							
Dissociation scheme	vac	C1	C2	C3	C4	C5	C6	C7
2H2 − C4in − C0up → (2H2 − C4in) + C0	+10.77	+1.01	+1.77	+3.32	+4.91	−0.76	−2.80	+0.16
2H2 − C4in − C0up → (2H2 − C0up) + C4	+9.45	−2.74	−1.81	+0.10	+2.07	−3.98	−6.03	−2.68
2H2 − C4up − C0in →(2H2 − C0in) + C4	+13.25	+0.66	+1.67	+3.71	+5.80	−0.37	−2.41	+1.04
2H2 − C4up − C0in → (2H2 − C4up) + C0	+9.51	−4.06	−2.92	−0.63	+1.67	−4.72	−6.76	−3.08
2H1 − C0up − C0do → (2H1 − C0up) + C0	+9.02	−2.41	−1.46	+0.45	+2.37	−3.63	−5.68	−2.45

5 that it would be possible to find (*T*,*P*) conditions where experiments and theoretical predictions qualitatively agree. A third hypothesis is to be brought to the forefront by the following observation.

One experimental fact worth mentioning is that, in all the mass spectra, the peak corresponding to the monoprotonated ligand alone is very weak compared to that corresponding to the biprotonated one. It is plausible to imagine that the main component of the ligand population in solution is found in its biprotonated state. Thus, all the complexes with the diacids, be they dimers or trimers, would be primarily formed with the biprotonated ligand. According to the different pKa's of the diacids, the population of their different protonated or deprotonated states will vary. One might suppose that there exists a sufficient proportion of undissociated diacid to provide $(\boldsymbol{L} + \boldsymbol{Cn} + 2\mathrm{H})^{2+}$, but there can also be enough monoanionic $(\boldsymbol{Cn} - \mathrm{H})^{-}$ species to lead to $(\boldsymbol{L} + \boldsymbol{Cn} - \mathrm{H})^{+}$. The geometry optimization of the complex $(\boldsymbol{L} + 2\mathrm{H}^{+} + \boldsymbol{C0}^{-}\boldsymbol{up})$ was performed at the B_3LYP level; this complex is characterized by a ΔE_{int} of −146 kcal/mol. This value is very important. Nevertheless, it drops down to −29.52 kcal/mol when the solvent effect is taken into account via the so-called IPCM model [26]. Thus, the difference in the solvation energies of the charged (2+, −, +) species involved clearly plays an important role. Another possibility is that, due to the pKa of ***Cn***, the complex $(\boldsymbol{L} + \boldsymbol{Cn} + 2\mathrm{H})^{2+}$ loses one proton.

The mixed trimer complexes $(\boldsymbol{L} + \boldsymbol{C0} + \boldsymbol{C4} + 2\mathrm{H})^{2+}$ are somewhat intriguing. The MS/MS experiments reveal that ***C0*** is always the first to leave the association. From the few theoretically studied complexes, this happens only when ***C0*** occupies the ***in*** position (Table 9) which is the least stable one in all the investigated complexes. The dissociation free energies $\Delta_d G$ are qualitatively similar for both ***C0*** and ***C4*** at the ***in*** position. However, the trimer $(\boldsymbol{L} + \boldsymbol{C4up} + \boldsymbol{C0in} + 2\mathrm{H})^{2+}$ seems to be slightly less stable than $(\boldsymbol{L} + \boldsymbol{C4in} + \boldsymbol{C0up} + 2\mathrm{H})^{2+}$ for a large set of (*T*,*P*) conditions (Tables 5 and 8). Thus, it is probable that other complexes are formed that would be more abundant that those studied. This proposal is enforced by the data on the trimer noted (***2H1 − C0up − C0do***) (Tables 5 and 9) which suggest that such associations could be more probable than the others while presenting similar $\Delta_d G$ as the cases of ***Cn in*** leaving partners.

Table 10. Interaction energies ΔE_{int} (kcal/mol) calculated for the dimers ***H2 − C0in*** and ***H2 − C2fin*** and for the trimer ***2H1 − C0up − C0in***, at the semiempirical AM1 and ab initio levels, for two optimized geometries (AM1 and ab initio). For the trimer, two dimer interactions were considered: the first one implies the ***2H1 − C0up*** complex on one hand and ***C0in*** on the other; the second one considers the ***2H1 − C0in*** complex in front of ***C0up***

Interacting partners	Calculation level	Optimized geometry	ΔE_{int}
H2 − C0in	AM1	AM1	−12.12
	RHF/MINI-1′	AM1	−13.32
H2 − C2fin	AM1	AM1	−10.34
	RHF/MINI-1′	AM1	−8.50
(***2H1 − C0up***) + ***C0in***	AM1	AM1	−8.493
	B3LYP/6-31G	AM1	−10.041
	B3LYP/6-31G	B3LYP/6-31G	−23.342
(***2H1 − C0in***) + ***C0up***	AM1	AM1	−16.054
	B3LYP/6-31G	AM1	−20.306
	B3LYP/6-31G	B3LYP/6-31G	−24.579
2H1 + C0up + C0in	AM1	AM1	−25.287
	B3LYP/6-31G	AM1	−31.590
	B3LYP/6-31G	B3LYP/6-31G	−48.361

Conclusions

Quantum chemistry calculations constitute a useful tool for proposing several probable conformations of the complexes observed in mass spectrometry, in view of their relative stabilities. The semiempirical level (AM1) mostly used in this work provides qualitative information about the investigated complexes. Moreover, the influence of the temperature and pressure conditions have also been addressed through quantum chemistry calculations. The main problem for comparing theoretical and experimental results is that the temperature and pressure conditions under which the mass spectra are recorded are not defined, even if some assumptions can be proposed. Nevertheless, the theoretical calculations indicate how these external conditions can influence the complex's fate.

Good agreement is observed between theoretical and experimental results with the ***C2m*** and ***C2f*** complexes, as well as for the biprotonated dimer and trimer with ***C0***. In contradiction, a disagreement appears between theoretical and experimental results concerning the

monoprotonated complexes with ***C2f*** and ***C0*** and for the dissociation of the mixed trimers with ***C0*** and ***C4***. These discrepancies could be explained by the fact that only some conformations have been investigated in this work and that other arrangements could exist with a lower energy. Nevertheless, even if the whole conformational space is not accessible to the study, it clearly appears that the combination of quantum chemistry calculations and electrospray mass spectrometry experiments could provide very useful information about the different ionic noncovalent complexes formed.

Acknowledgments

This work was supported in part by the Belgian program on Interuniversity Poles of Attraction initiated by the Belgian State, Prime Minister's Office, *Service fédéraux des affaires scientifiques, techniques et culturelles* (PAI no P4/03), the *Fonds de la Recherche Scientifique Médicale* (contract no 3.4531.92) and by the pharmaceutical industrial group Servier-Adir. GD is *chercheur qualifié* of the FNRS, Brussels.

References

1. Lehn, J.-M. *Acc. Chem. Res.* **1978,** *11*, 49.
2. Park, C. H.; Simmons, H. E. *J. Am. Chem. Soc.* **1968,** *90*, 2431.
3. Kotzyba-Hibert, F.; Lehn, J.-M.; Vierling, P. *Tetrahedron Lett.* **1980,** *21*, 941.
4. Hosseini, M. W.; Lehn, J.-M. *J. Am. Chem. Soc.* **1982,** *3525*, 3527.
5. Kimura, E.; Sakonaka, A.; Yatsunami, T.; Kodama, M. *J. Am. Chem. Soc.* **1981,** *103*, 3041.
6. Dietrich, B.; Hosseini, M. W.; Lehn, J.-M.; Sessions, R. B. *J. Am. Chem. Soc.* **1981,** *103*, 1282.
7. Pócsfalvi, G.; Lipták, M.; Huszthy, P.; Bradshaw, J. S.; Izatt, R. M.; Vékey, K. *Anal. Chem.* **1996,** *68*, 792.
8. Sawada, M.; Takai, Y.; Yamada, H.; Hirayama, S.; Kaneda, T.; Tanaka, T.; Kamada, K.; Mizooku, T.; Takeuchi, S.; Ueno, K.; Hirose, K.; Tobe, Y.; Naemura, K. *J. Am. Chem. Soc.* **1995,** *117*, 7726.
9. Vincenti, M. *J. Mass Spectrom.* **1995,** *30*, 925.
10. Abdoul-Carime, H. *J. Chem. Soc. Faraday Trans.* **1998,** *94*, 2407.
11. Jaquinot, M.; Leize, E.; Potier, N.; Albrecht, A.-M.; Shanzer, A.; Van Dorsselaer, A. *Tetrahedron Lett.* **1993,** *34*, 2771.
12. Romero, F.; Ziessel, R.; Dupont-Gervais, A.; Van Dorsselaer, A. *Chem. Commun.* **1996**, 551.
13. Young, D.-S.; Hung, H.-Y.; Liu, L. K. *Rapid Commun. Mass Spectrom.* **1997,** *11*, 769.
14. Leize, E.; Jaffrezic, A.; Van Dorsselaer, A. *J. Mass Spectrom.* **1996,** *31*, 537.
15. Wang, K.; Gokel, G. W. *J. Org. Chem.* **1996,** *61*, 4693.
16. Collette, C.; Meunier, C.; De Pauw, E.; Dumont, A.; Desreux, J. F. *Rapid Commun. Mass Spectrom.* **1997,** *11*, 1521.
17. Dive, G.; Dehareng, D.; Peeters, D. Int. *J. Quantum Chem.* **1996,** *58*, 85.
18. Vancampenhout, N.; Dive, G.; Dehareng, D. *Int. J. Quantum Chem.* **1996,** *60*, 911.
19. McQuarrie, D. A. *Statistical Thermodynamics*; Harper and Row: New York, 1973.
20. Dewar, M. J. S.; Zoebisch, E. G.; Healy, E. F. *J. Amer. Chem. Soc.* **1985,** *107*, 3902.
21. Frisch, M. J.; Trucks, G. W.; Schlegel, H. B.; Gill, P. M. W.; Johnson, B. G.; Robb, M. A.; Cheeseman, J. R.; Keith, T. A.; Petersson, G. A.; Montgomery, J. A.; Raghavachari, K.; Al-Laham, M. A.; Zakrzewski, V. G.; Ortiz, J. V.; Foresman, J. B.; Cioslowski, J.; Stefanov, B. B.; Nanayakkara, A.; Challacombe, M.; Peng, C. Y.; Ayala, P. Y.; Chen, W.; Wong, M. W.; Andres, J. L.; Replogle, E. S.; Gomperts, R.; Martin, R. L.; Fox, D. J.; Binkley, J. S.; Defrees, D. J.; Baker, J.; Stewart, J. P.; Head-Gordon, M.; Gonzalez, C.; and Pople, J. A. Gaussian 94 (Revision D.4), Gaussian Inc., Pittsburgh PA, 1996.
22. Tatewaki, H.; Huzinaga, S. *J. Comp. Chem.* **1980,** *1*, 205.
23. Dive, G.; Dehareng, D.; Ghuysen, J. M. *Theor. Chim. Acta* **1993,** *85*, 409.
24. Becke, A. D. *J. Chem. Phys.* **1993,** *98*, 5648.
25. Hehre, W. J.; Ditchfield, R.; Pople, J. A. *J. Chem. Phys.* **1972,** *56*, 2257.
26. Foresman, J. B.; Keith, T. A.; Wiberg, K. B.; Snoonian, J.; Frisch, M. J. *J. Phys. Chem.* **1996,** *100*, 16098.
27. Miertus, S.; Scrocco, E.; Tomasi, J. *Chem. Phys.* **1981,** *55*, 117.
28. Copyright 1993, Biosym Technologies, Inc., 9685 Scranton Road, San Diego, CA 92121-2777, USA.
29. CFF91 forcefield used by the Discover program from Biosym Technologies, [28]. Results available upon request.